Loading Behavior of {Chitosan/Hyaluronic Acid}$_n$ Layer-by-Layer Assembly Films toward Myoglobin: An Electrochemical Study

Haiyun Lu and Naifei Hu*

Department of Chemistry, Beijing Normal University, Beijing 100875, China

Received: June 7, 2006; In Final Form: September 18, 2006

When {CS/HA}$_n$ layer-by-layer films assembled by oppositely charged chitosan (CS) and hyaluronic acid (HA) were immersed in myoglobin (Mb) solution at pH 5.0, Mb was gradually loaded into the {CS/HA}$_n$ films, designated as {CS/HA}$_n$−Mb. The cyclic voltammetric (CV) peak pair of Mb Fe^{III}/Fe^{II} redox couple for {CS/HA}$_n$−Mb films on pyrolytic graphite (PG) electrodes was used to investigate the loading behavior of {CS/HA}$_n$ films toward Mb. The various influencing factors, such as the number of bilayers (n), the pH of Mb loading solution, and the ionic strength of solution, were investigated by different electrochemical methods and other techniques. The results showed that the main driving force for the bulk loading of Mb was most probably the electrostatic interaction between oppositely charged Mb in solution and HA in the films, while other interactions such as hydrogen bonding and hydrophobic interaction may also play an important role. Other polyelectrolyte multilayer (PEM) films with different components were compared with {CS/HA}$_n$ films in permeability and Mb loading, and electroactive probes with different size and surface charge were compared in their incorporation into PEM films. The results suggest that due to the unique structure of CS and HA, {CS/HA}$_n$ films with relatively low charge density are packed more loosely and more easily swelled by water, and have better permeability, which may lead to the higher loading amount and shorter loading time for Mb. The protein-loaded PEM films provide a new route to immobilize redox proteins on electrodes and realize the direct electrochemistry of the proteins.

Introduction

The effective immobilization of enzymes on solid substrates without changing the original conformations and bioactivities of the enzymes has attracted increasing interest among researchers along with rapid advances of biotechnology and biodevices. Since the 1990s, a novel layer-by-layer assembly technique mainly based on alternate adsorption of oppositely charged species on solid surfaces has been developed.[1] This approach can be used to fabricate ultrathin polyelectrolyte multilayer (PEM) films according to a predesigned architecture with precise thickness control. The layer-by-layer assembly has now been extended to constructing protein films with oppositely charged polyions or nanoparticles,[2] and the direct electrochemistry of some redox proteins in these multilayer films on electrodes has also been realized.[3,4] The study of direct electron transfer of proteins with underlying electrodes can provide a model for the mechanistic study of electron transfer between enzymes in real biological systems and establish a foundation for fabricating a new type of biosensor, bioreactor, and biomedical device without using mediators.[5,6]

Recently, PEM films have been used as a matrix for incorporation of proteins. When PEM films assembled on solid substrates are immersed into protein solutions, under suitable conditions, the protein can not only be adsorbed onto the surface of films but also be loaded or "absorbed" into the films.[7−9] For example, Schlenoff and co-worker studied the adsorption/absorption mechanism of different proteins onto/into PEMs.[7] When the surface charges of PEM and proteins were opposite, PEM films could act as a "sponge" to absorb or load the proteins into the films. Weidinger et al. investigated the redox processes of cytochrome *c* (Cyt-c) immobilized in PEM films.[9] For PEI/PSS/{PAH/PSS}$_n$ films, where PEI is poly(ethyleneimine), PSS is poly(styrenesulfonate), and PAH is poly(allylamine hydrochloride), positively charged Cyt-c could be loaded inside the PEM films, accompanied by the formation of a PSS/Cyt-c complex and rearrangement of the layered structure. PEM films have also been used to fabricate hollow microcapsules. In the procedure, the layer-by-layer assembly of the PEM shell onto the surface of the colloidal microtemplate core is followed by the decomposition and removal of the solid core under suitable conditions. The controllable loading of proteins into the PEM capsules and then the release of proteins out of the microcapsules have been reported.[10]

The protein-loaded PEM films based on layer-by-layer assembly are easy-to-made and well controllable. Since the loading of proteins is established on the basis of spontaneous adsorption or/and absorption of the proteins, the native structure and biological activity of entrapped proteins in the PEM films can be retained.[11] This inspired us to use this method to immobilize redox proteins or enzymes and to design biosensors and bioreactors based on the direct electrochemistry of proteins at the protein-loaded PEM film electrodes. However, the loading process of PEM films toward proteins is usually extremely slow and time-consuming, and the immobilization amount of proteins is often very limited, mainly because of the poor permeability of most PEM films and the relatively large size of proteins. Only those PEM films with appropriate constituents and suitable structure can demonstrate good permeability toward some specific proteins and effectively load the proteins. PEM films

* Corresponding author. Tel.: +86 10 5880 5498. Fax: +86 10 5880 2075. E-mail: hunaifei@bnu.edu.cn.

10.1021/jp063550d CCC: $33.50
Published on Web 11/09/2006

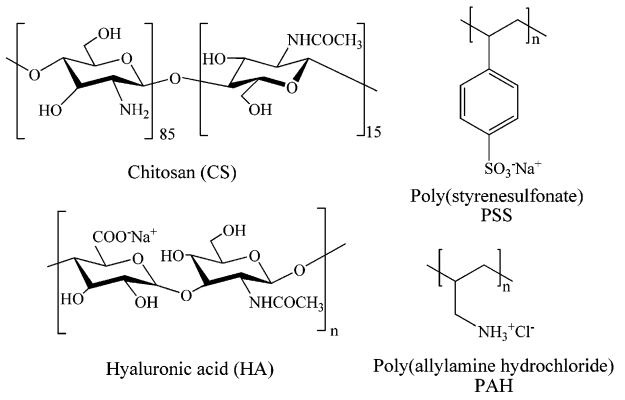

Figure 1. Chemical structures of the polyelectrolytes used in this work.

assembled by different polyelectrolyte constituents with different charge density and structure exhibit different properties in solute permeability, water swelling, species separation, and nanofiltration.[12−14] Generally, PEM films prepared with polyelectrolytes of low charge density show high swelling and fast solute transport because of a low degree of ionic cross-linking in the films.[12]

In the present work, natural polysaccharides chitosan (CS) and hyaluronic acid (HA) were selected as the building components of PEM films. The chemical structures of CS and HA are shown in Figure 1. Both CS and HA are weak polyelectrolytes with good biocompatibility, nontoxicity, and biodegradability and have been widely used in pharmaceutical applications,[15] tissue engineering, drug delivery,[16,17] and others. The $\{CS/HA\}_n$ layer-by-layer films have also been studied and used in many applications in recent years.[8,12a,b,18−23] For example, Bruening and co-workers studied the correlation of the swelling and permeability of PEM films.[12a] In their work, with high swelling capacity and good permeability, the $\{CS/HA\}_n$ films were used in the separation of different saccharides and isolation of sugar from salt solutions. It was reported that the $\{CS/HA\}_n$ films were highly permeable for some low molecule-weight proteins, such as myoglobin (Mb), and were used to fractionate proteins[12b] and to immobilize trypsin in digesting proteins.[8] Particularly, $\{CS/HA\}_n$ layer-by-layer films demonstrated an exponential-growth behavior,[12b,19,20] which was different from the linear-growth mode for most PEM films. This type of PEM film was believed to be loosely packed and rather porous, as compared to the densely packed and ordered structure of linearly growing PEM films.[24,25]

We therefore expected that Mb would be easily and effectively loaded into the $\{CS/HA\}_n$ multilayer films from its solution, forming Mb-loaded PEM films, designated as $\{CS/HA\}_n$−Mb. Herein, Mb was selected as the model protein because of its well-known structure and properties, commercial availability, and relatively small size. Particularly, the good and direct electrochemistry of Mb in cast Mb-CS films[26] and $\{Mb/HA\}_n$ layer-by-layer films[27] has been realized. All these may make Mb become a good electroactive probe in the study of loading behavior of $\{CS/HA\}_n$ films. Different electrochemical approaches, such as cyclic voltammetry (CV), electrochemical impedance spectroscopy (EIS), and rotating disk voltammetry (RDV), and other techniques including quartz crystal microbalance (QCM), UV−vis spectroscopy, and scanning electron microscopy (SEM), were used to characterize the $\{CS/HA\}_n$ and $\{CS/HA\}_n$−Mb films. The possible mechanism and driving forces of Mb incorporation into the films were explored by studying the influence of various factors. To further understand the relationship between the structure feature and permeation property of PEM films, $\{CS/PSS\}_n$ and $\{PAH/PSS\}_n$ layer-by-layer films were also assembled, and the loading behavior of these films toward Mb was compared with that of $\{CS/HA\}_n$ films. The chemical structures of PAH and PSS are also shown in Figure 1. Other heme proteins with larger size, hemoglobin (Hb) and catalase (Cat), and some small molecules or ions such as hemin, ferrocenecarboxylic acid (Fc(COOH)), $Fe(CN)_6^{3-/4-}$, and $Ru(NH_3)_6^{3+}$, were also used as electroactive probes to investigate the permeability of the films. The profound understanding of permeability and loading behavior of PEM films toward proteins may guide us to find more suitable polyelectrolytes in the future and to fabricate the layer-by-layer films that can demonstrate better loading property toward proteins. To the best of our knowledge, only a few studies have been reported on loading behavior of PEM films toward proteins up to now.[7−9]

Experimental Section

1. Chemicals. Horse heart myoglobin (Mb, MW 17 800), bovine hemoglobin (Hb, MW 66 000), bovine liver catalase (Cat, 15 000 units mg^{-1}, MW 240 000), hemin, and chitosan (CS, the degree of acetylation is less than 15%, MW ∼ 200 000) were purchased from Sigma. Poly(allylamine hydrochloride) (PAH, MW ∼ 70 000), poly(styrenesulfonate) (PSS, MW ∼ 70 000), 3-mercapto-1-propanesulfonate (MPS), and ferrocenecarboxylic acid (Fc(COOH)) were purchased from Aldrich. Hyaluronic acid (HA, MW ∼ 400 000) was purchased from Fluka. Hexaammineruthenium(III) chloride ($Ru(NH_3)_6Cl_3$) was obtained from Alfa Aesar. $K_3Fe(CN)_6$ and $K_4Fe(CN)_6$ were obtained from Beijing Chemical Plant. All other chemicals were reagent grade. All solutions were prepared with twice-distilled water.

2. Film Assembly. For assembly of PEM or {polycation/polyanion}$_n$ films on electrodes, clean and rough basal plane pyrolytic graphite disk (PG, Advanced Ceramics, geometric area 0.16 cm^2) electrodes were first immersed in positively charged CS (1 mg mL^{-1} at pH 5.0, containing 0.1 M NaCl) or PAH (3 mg mL^{-1}, containing 0.2 M NaCl) solutions for 20 min, and after being washed with water, the electrodes were then placed in negatively charged HA (1 mg mL^{-1} at pH 5.0, containing 0.1 M NaCl) or PSS (3 mg mL^{-1}, containing 0.2 M NaCl) solutions for 20 min. This cycle was repeated to fabricate $\{CS/HA\}_n$, $\{CS/PSS\}_n$, or $\{PAH/PSS\}_n$ layer-by-layer films on the PG surface with a desired number of bilayers (n). For Mb loading, the PEM film electrodes were usually immersed in 1 mg mL^{-1} Mb solution at pH 5.0 containing 0.5 M NaCl for a certain time. The Mb-loaded PEM films are designated as, for example $\{CS/HA\}_n$−Mb. The $\{CS/HA\}_n$−Mb films were then transferred in pH 7.0 buffers (0.05 M KH_2PO_4 + 0.05 M KBr, ionic strength 0.1 M) containing no Mb, and CV was performed.

For QCM studies, gold QCM electrodes (geometric area 0.196 cm^2, fundamental frequency 8 MHz) were first pretreated with piranha solution (3:7 volume ratio of 30% H_2O_2 and 98% H_2SO_4. Caution: the piranha solution should be handled with extreme care, and only small volumes should be prepared at any time). After being washed with water thoroughly, the Au electrodes were immersed in MPS solution (4 mM) for 24 h to chemisorb an MPS monolayer and make the surface become negatively charged. The $\{CS/HA\}_n$ and $\{CS/HA\}_n$−Mb films were then assembled on the Au/MPS surface with the same procedure as that used on the PG electrodes. Before and after the loading of Mb, the QCM electrodes were washed with water and dried under a nitrogen stream, and the frequency was measured by QCM in air.

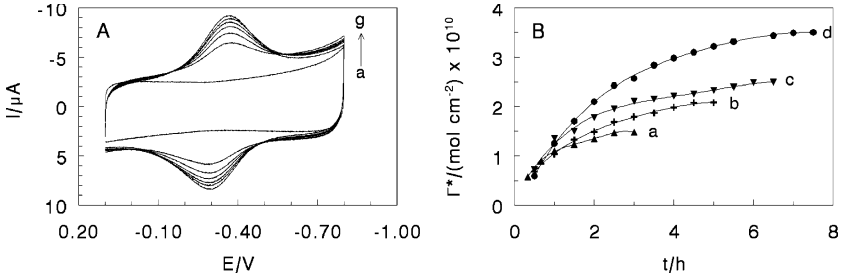

Figure 2. (A) Cyclic voltammograms in pH 7.0 buffers at 0.2 V s^{-1} for $\{CS/HA\}_7$−Mb films after the $\{CS/HA\}_7$ film electrodes were immersed in 1 mg mL^{-1} Mb solution at pH 5.0 for (a) 0, (b) 1, (c) 2, (d) 3, (e) 4, (f) 5, and (g) 7 h. (B) Effect of the immersing time in Mb solution on the surface concentration of electroactive Mb (Γ*) for $\{CS/HA\}_n$−Mb films with different number of bilayers (n): (a) $n = 1$, (b) $n = 3$, (c) $n = 5$, and (d) $n = 7$.

3. Apparatus. A CHI 660A electrochemical workstation (CH Instruments) was used for all electrochemical measurements at ambient temperature (20 ± 2 °C). A saturated calomel electrode (SCE) was used as the reference, a platinum wire as the counter electrode, and the PG disk electrode with films as the working electrode. In CV studies, buffers were purged with high-purity nitrogen for at least 15 min prior to measurements, and a nitrogen environment was maintained during the CV scans. For RDV experiments, a rotator and speed controller (Pine Instruments) were utilized. EIS was performed in the presence of 5 mM $K_4Fe(CN)_6/K_3Fe(CN)_6$ (1:1, containing 0.1 M KCl). A sinusoidal potential modulation with amplitude of ±5 mV was superimposed on the formal potential of the redox couple of $Fe(CN)_6^{4-/3-}$ (0.17 V vs SCE), and the applied frequency was from 10^5 to 0.1 Hz.

QCM was performed with a CHI 420 electrochemical analyzer. Based on the Sauerbrey equation,[28] $\Delta F = -2F_0^2A^{-1}(\mu\rho_0)^{-1/2}\Delta m$, where F_0 is resonant frequency of the fundamental mode of the quartz crystal (8 MHz), μ is the shear modulus of quartz (2.947×10^{11} g cm^{-1} s^{-2}), ρ_0 is the density of the crystal (2.648 g cm^{-3}), and A is the geometric area of the QCM electrode (0.196 cm^2), the frequency shift, ΔF (Hz), would be proportional to the adsorbed mass, Δm (g), by taking into account the properties of quartz resonator used in this work. Thus, a 1 Hz of frequency decrease corresponds to 1.35 ng of mass increase. The surface concentration of loaded Mb in $\{CS/HA\}_n$ films (Γ, mol cm^{-2}) can then be estimated based on Δm after the loading. The viscoelastic effect in QCM measurement that is significant in solution can be ignored when the QCM measurement is performed in air for a dry and rigid adsorption layer. In this case, the Sauerbrey equation is reliable as also shown in previous studies.[29,30]

A Cintra 10e UV−visible spectrophotometer (GBC) was used for UV−vis spectroscopy. SEM was performed with a Hitachi S-4800 field emission scanning electron microscope with an acceleration voltage of 5 kV.

Results

1. Loading of Mb into $\{CS/HA\}_n$ Layer-by-Layer Assembly Films. CS is a weak polybase and its conjugated acid has pK_a at about 6,[31] and HA is a weak polyacid with pK_a = 2.9.[15] Thus, at pH 5.0, positively charged CS and negatively charged HA can be alternatively adsorbed on the electrode surface via electrostatic interaction between them, forming $\{CS/HA\}_n$ layer-by-layer films. The films showed an exponential growth of the film mass and thickness with the number of deposited layers under suitable conditions.[12b,19,20,27]

With the isoelectric point at 6.8,[32] Mb has net positive surface charges at pH 5.0. It was found that Mb in pH 5.0 buffers could be loaded into the $\{CS/HA\}_n$ films,[12b] forming $\{CS/HA\}_n$−Mb films. The process of protein loading was monitored by CV in the present work. For example, after $\{CS/HA\}_7$ films with $n = 7$ assembled on PG electrodes were immersed in Mb solution for a certain time, the resulting $\{CS/HA\}_7$−Mb film electrodes were transferred in pH 7.0 buffers containing no protein and then tested by CV. A well-defined, quasireversible reduction−oxidation peak pair was observed at about −0.34 V vs SCE, characteristic of Mb heme Fe^{III}/Fe^{II} redox couple,[33] and the peak currents increased with the immersing time in Mb solution (Figure 2A). In the meantime, $\{CS/HA\}_7$ films containing no protein at PG electrodes gave no CV response at all in the same potential range (Figure 2A, curve a). For a specific $\{CS/HA\}_n$−Mb film with a certain n value and particular immersing time, CVs showed nearly symmetric peak shapes and roughly equal heights of reduction and oxidation peaks, and the peak currents increased linearly with scan rates from 0.05 to 2.0 V s^{-1}, indicating the diffusionless and surface-confined voltammetric behavior.[34] In this case, integration of CV reduction peak would give the charge (Q) for full reduction of electroactive Mb in the films, and the Q value could be further converted to the surface concentration of electroactive Mb (Γ*, mol cm^{-2}) in the films. The dependence of Γ* on immersing time (t) for $\{CS/HA\}_n$−Mb films with different n values showed the similar tendency, in which Γ* initially increased with t, and then tended to level off and did not increase with t any more (Figure 2B). If Γ^*_{max} was defined as the maximum surface concentration of electroactive Mb when the Γ* reached the steady state for a $\{CS/HA\}_n$−Mb film, and t_{max} was defined as the immersing time when Γ* began to reach the steady state, both Γ^*_{max} and t_{max} values increased with the number of bilayers (n). This is understandable since thicker $\{CS/HA\}_n$ films would load and accommodate more Mb, and the incorporated Mb would take longer time to reach the equilibrium or the steady state.

The $\{CS/HA\}_n$−Mb films displayed excellent stability in blank buffers containing no Mb. For example, after one month of storage in pH 5.0 or 7.0 buffers at ambient temperature, the fully loaded $\{CS/HA\}_5$−Mb film electrodes showed CV peaks at the same potential as that at their initial steady state with no obvious decrease in peak currents.

2. Influencing Factors on Loading of Mb into $\{CS/HA\}_n$ Films. Various factors, such as the number of bilayers (n), the pH of Mb loading solution, and the ionic strength of Mb loading solution and "exposure" solution, affected the loading behavior of $\{CS/HA\}_n$ films toward Mb. The influence of the number of bilayers (n) on Γ^*_{max} measured by CV and Γ_{max} estimated by QCM at the same t_{max} for $\{CS/HA\}_n$−Mb films was first investigated (Figure 3). The results demonstrated that at the same n, Γ^*_{max} was always smaller than Γ_{max}, indicating that only a fraction of Mb molecules loaded in the films is electrochemically accessible. In addition, while the total amount of Mb loaded

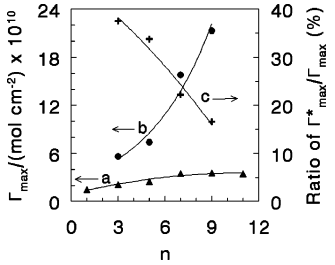

Figure 3. Influence of the number of bilayers (n) of $\{CS/HA\}_n$−Mb films on (a) the maximum surface concentration of electroactive Mb (Γ^*_{max}) measured by CV in pH 7.0 buffers at t_{max} and 0.2 V s^{-1}, (b) the surface concentration of Mb (Γ_{max}) measured by QCM at the same t_{max}, and (c) the ratio of $\Gamma^*_{max}/\Gamma_{max}$.

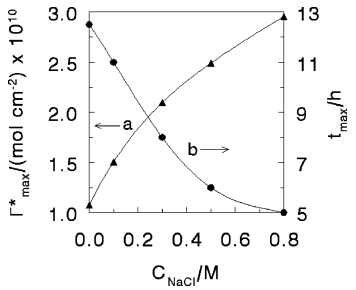

Figure 4. Influence of the NaCl concentration in Mb loading solution on (a) the maximum surface concentration of electroactive Mb (Γ^*_{max}) and (b) the corresponding loading time (t_{max}) for $\{CS/HA\}_5$−Mb films measured by CV in pH 7.0 buffers at 0.2 V s^{-1}.

into $\{CS/HA\}_n$ films at t_{max} (Γ_{max}) increased with n, the maximum surface concentration of electroactive Mb (Γ^*_{max}) could just increase with n up to 7 and did not increase with n any more when $n > 7$. The fraction of electroactive Mb ($\Gamma^*_{max}/\Gamma_{max}$) in the films showed an obvious decreasing tendency with n (Figure 3).

The pH of the Mb loading solution, which decided the net surface charge of Mb, had a significant influence on the loading amount of Mb in $\{CS/HA\}_n$ films. CVs of $\{CS/HA\}_3$−Mb films showed that the amount of electroactive Mb loaded at pH 5.0 was much larger than that of Mb loaded at pH 7.0 or 9.0 (Supporting Information Figure S1A). This situation had little relationship with the charge of outermost layer for the films. As Figure S1B displayed, even when the outermost layer was positively charged CS, the CV peak currents or the loading amount of electroactive Mb for $\{CS/HA\}_3$/CS−Mb films loaded at pH 5.0 were still much larger than those for the films loaded at pH 7.0 or 9.0. Figure S1 presents CVs of $\{CS/HA\}_3$−Mb and $\{CS/HA\}_3$/CS−Mb films prepared from the Mb loading solution at different pH and with different t_{max}. For example, for $\{CS/HA\}_3$−Mb films, the t_{max} value was 4.5 h at pH 5.0, 24 h at pH 9.0, and 24 h at pH 7.0. The t_{max} values for the films loaded at pH 5.0 were much smaller than those for the corresponding films loaded at pH 7.0 or 9.0, suggesting that it is much easier for positively charged Mb at pH 5.0 to "absorb" into the films than at other pHs, irrelative to the surface charge situation of the PEM films.

The ionic strength or the concentration of NaCl in the Mb loading solution greatly influenced the loading behavior of $\{CS/HA\}_n$ films. When the ionic strength of Mb loading solution increased, the Γ^*_{max} increased accordingly, and the corresponding loading time (t_{max}) decreased (Figure 4). The ionic strength of "exposure" solution also affected the electrochemical activity of Mb in $\{CS/HA\}_n$−Mb films modified on electrode surface. For example, Mb-loaded $\{CS/HA\}_3$ films at the steady state were placed into the "exposure" solution with different concentrations of NaCl for 2 h and then transferred into pH 7.0 buffers and tested by CV (Supporting Information Figure S2). The results demonstrated that the Γ^* of $\{CS/HA\}_3$−Mb films increased with the NaCl concentration of exposure solution. Since the total amount of Mb in the $\{CS/HA\}_3$−Mb films would not increase during the exposure, and only a fraction of Mb loaded in the films is electroactive (Figure 3), the increase of Γ^* with the NaCl concentration of exposure solution suggests the increase of the fraction of electroactive Mb.

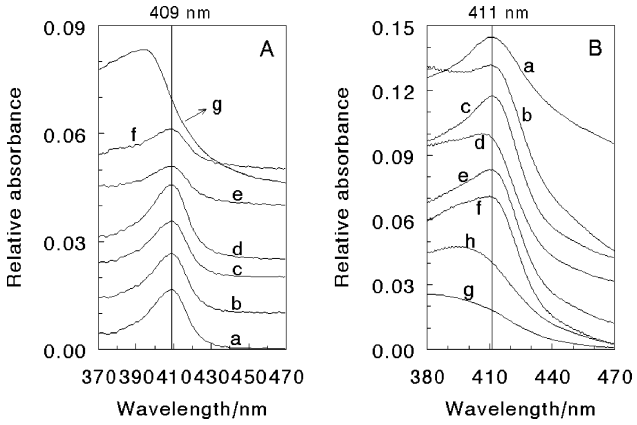

Figure 5. (A) UV−vis spectra of 1.1×10^{-7} M Mb in pH 7.0 buffers containing (a) 0, (b) 0.5, (c) 0.8, (d) 1, (e) 1.5, (f) 2 M NaCl, and (g) 1.8×10^{-6} M hemin in pH 7.0 buffers. (B) UV−vis spectra on quartz slides for (a) dry Mb films, (b) dry $\{CS/HA\}_9$−Mb films, and $\{CS/HA\}_9$−Mb films in buffers at different pH: (c) pH 7.0, (d) pH 5.0, (e) pH 9.0, (f) pH 12.0, (g) pH 3.0, and (h) dry $\{CS/HA\}_9$−hemin films.

Another important factor that affected the loading behavior of Mb into $\{CS/HA\}_n$ films would be the molecular weights of CS and HA. According to Badia and co-workers,[19b] the thickness of $\{CS/HA\}_n$ films depended on the size of both CS and HA, and the films assembled by polysaccharides with higher molecular weights were thicker than those with lower molecular weights. We thus expect that the thicker $\{CS/HA\}_n$ films with longer CS and HA polymer chains would incorporate more amounts of Mb than that of the thinner films with lower polysaccharide molecular weights under the same conditions. The study on the influence of polymer chain lengths will be performed in the future in our laboratory.

3. Conformational Study of $\{CS/HA\}_n$−Mb Films. The Soret absorption spectroscopic band of heme proteins may provide information on conformational integrity of the proteins, especially in their heme region.[35] To investigate the influence of ionic strength on Mb conformation, a series of Mb solutions with different NaCl concentrations was prepared, and the UV−vis spectra were measured after 24 h (Figure 5A). Mb in NaCl solutions of ≤2 M showed the Soret band at 409 nm, almost the same as that of Mb in pure water, indicating that Mb retains its near-native conformation even in 2 M NaCl solution. For comparison, hemin, a free heme group, showed the Soret band at 395 nm in solution. The obvious blue shift of Soret band for hemin compared with Mb suggests that the heme prosthetic group of Mb does not split out from Mb polypeptide matrix. The Soret band position of Mb in different Mb films was also investigated by UV−vis spectroscopy (Figure 5B). Both dry Mb and $\{CS/HA\}_9$−Mb films on quartz slides showed the Soret band at 411 nm, suggesting that Mb incorporated in $\{CS/HA\}_9$ films keeps a near-native structure as that in dry Mb films alone. The Soret band position depended on the pH of external buffer solution in which the $\{CS/HA\}_9$−Mb films were immersed. At pH between 5.0 and 12.0, the Soret band was observed at 411 nm, the same as that of dry Mb and $\{CS/HA\}_9$−Mb films,

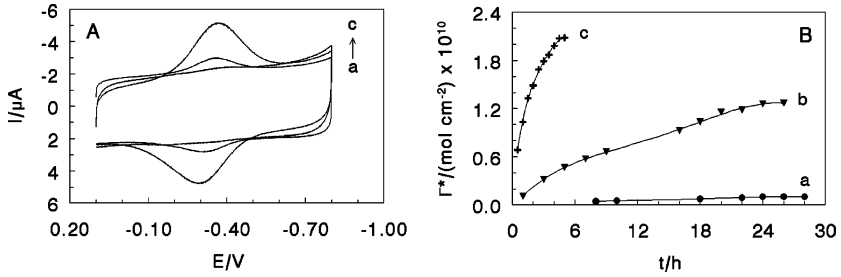

Figure 6. (A) Cyclic voltammograms in pH 7.0 buffers at 0.2 V s^{-1} for (a) {PAH/PSS}$_3$−Mb, (b) {CS/PSS}$_3$−Mb, and (c) {CS/HA}$_3$−Mb films after the multilayer films were immersed in 1 mg mL^{-1} Mb solution at pH 5.0 for 5 h. (B) Effect of the immersing time on the surface concentration of electroactive Mb (Γ*) for (a) {PAH/PSS}$_3$−Mb, (b) {CS/PSS}$_3$−Mb, and (c) {CS/HA}$_3$−Mb films measured by CV in pH 7.0 buffers at 0.2 V s^{-1}.

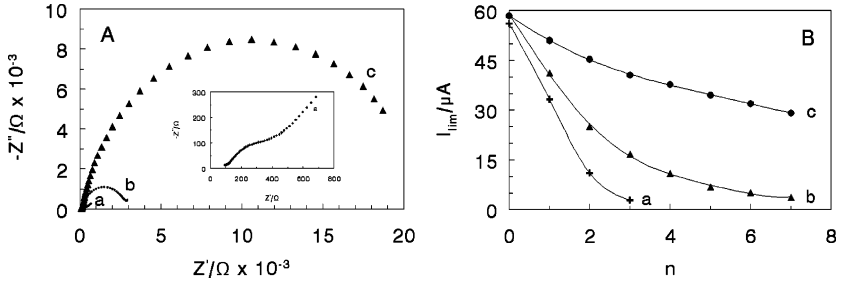

Figure 7. (A) Electrochemical impedance spectra of $Fe(CN)_6^{4-/3-}$ at 0.17 V for (a) {CS/HA}$_3$, (b) {CS/PSS}$_3$, and (c) {PAH/PSS}$_3$ films on PG electrodes. Inset is the amplified EIS spectrum of (a). (B) Influence of the number of bilayers (n) on RDV oxidation limiting current (I_{lim}) of 0.5 mM Fc(COOH) in pH 7.0 buffers at 0.2 V s^{-1} and 4000 rpm for (a) {PAH/PSS}$_n$, (b) {CS/PSS}$_n$, and (c) {CS/HA}$_n$ films on PG electrodes.

suggesting that Mb in {CS/HA}$_9$−Mb films essentially retains its native structure in a wide range of pH. When pH was changed to 3.0, the Soret band shifted to less than 400 nm and became distorted (Figure 5B, curve g), similar to that of dry {CS/HA}$_9$−hemin films (Figure 5B, curve h), indicating that Mb in the films may denature to a considerable extent at pH 3.0.

4. Comparison of {CS/HA}$_n$ Films with {CS/PSS}$_n$ and {PAH/PSS}$_n$ Films. To investigate the possible reason {CS/HA}$_n$ films had the good loading capability toward Mb, two other PEM films, {CS/PSS}$_n$ and {PAH/PSS}$_n$, were assembled on the PG surface, and their loading behavior toward Mb was compared with {CS/HA}$_n$ films. For example, with the same bilayer number of 3 and immersing time of 5 h, the CV peak currents of {CS/HA}$_3$−Mb films were much larger than those of {CS/PSS}$_3$−Mb films, while {PAH/PSS}$_3$−Mb films showed no CV response at all (Figure 6A). The great difference among the three PEM films in Mb loading was also displayed in Figure 6B. Compared with the other two PEM films, {CS/HA}$_3$ films demonstrated the best Mb loading capability. It is much easier for Mb to enter into {CS/HA}$_3$ films, go through the whole films, and exchange electrons with the electrodes.

The different Mb loading properties for the three PEM films are probably related to the difference in their permeability. EIS was thus performed to study the porosity of the three films with $Fe(CN)_6^{3-/4-}$ redox couple as the electroactive probe at its formal potential (0.17 V vs SCE). Figure 7A shows the EIS spectra in the form of Nyquist diagrams at different film electrodes. For {CS/HA}$_3$ films, the EIS response showed a Warburg line in a very wide frequency range, while a semicircle was obviously observed in the high-frequency domain for {CS/PSS}$_3$ and {PAH/PSS}$_3$ films, respectively. In addition, the diameter of the semicircle, which usually equals the electron-transfer resistance (R_{ct}) and reflects the electron-transfer rate of the redox probe at the electrode interface,[36] was quite different for the three multilayer films. Compared with {CS/PSS}$_3$ (2.6×10^3 Ω) and {PAH/PSS}$_3$ films (1.9×10^4 Ω), {CS/HA}$_3$ films showed the smallest R_{ct} (3.9×10^2 Ω). In this particular case, to a much more extent, R_{ct} reflects the restricted diffusion of the probe through the layer system, and relates directly to the accessibility of the underlying electrode or the film permeability.[37] {CS/HA}$_n$ films thus showed the best permeability or highest porosity among the three films.

The porosity of three kinds of PEM films was also investigated by rotating disk voltammetry (RDV) using Fc(COOH) as the probe. Herein, RDV was used because compared with the stationary electrode, the rotating electrode would greatly accelerate the mass transportation of the probe in solution phase and amplify the permeation difference between different films. The well-defined sigmoidal RDVs at about 0.29 V for the $Fc(COOH)^+$/Fc(COOH) couple were observed at bare PG electrodes (not shown). When {CS/HA}$_n$, {CS/PSS}$_n$, or {PAH/PSS}$_n$ films were assembled on the PG surface, the $E_{1/2}$ value of Fc(COOH) remained at the same position, but the oxidation limiting currents (I_{lim}) decreased with the number of bilayers (n) (Figure 7B). This implies that while the PEM films have some pores or channels that allow the probe to go through the films and reach the electrode surface to transfer electrons, the films also have a considerable blocking effect to prevent the probe from approaching the electrode surface, especially when the films become thick. However, the decrease rate or tendency of I_{lim} with n for the three PEM films was different, demonstrating the sequence of {CS/HA}$_n$ < {CS/PSS}$_n$ < {PAH/PSS}$_n$, suggesting that {CS/HA}$_n$ films have better porosity and allow the probe to go through the films more easily.

The influence of ionic strength or KCl concentration in $Fe(CN)_6^{3-}$ solution on the permeability of the films was also studied by RDV, and the results showed the decreased tendency of reduction limiting current of $Fe(CN)_6^{3-}$ (I_{lim}) with the number of bilayers (n) similar to the Fc(COOH) system (Supporting Information Figure S3). For a certain kind of PEM film with a fixed n value, the increase of KCl concentration usually resulted in the increase of I_{lim}, especially when n was large enough. These results are consistent with those of Figure 4, in which the Mb loading amount in {CS/HA}$_n$ films increased with the ionic strength.

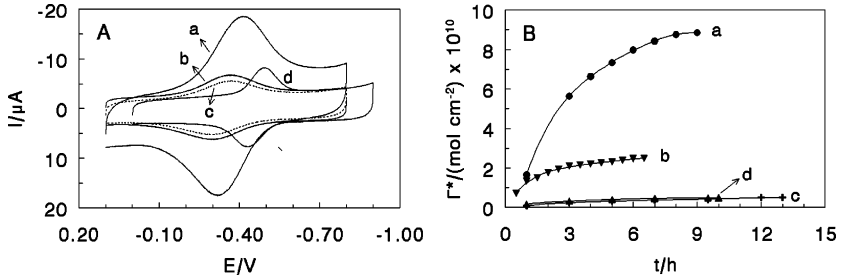

Figure 8. (A) Cyclic voltammograms in pH 7.0 buffers at 0.2 V s^{-1} for (a) $\{CS/HA\}_5$−hemin films after the $\{CS/HA\}_5$ films were immersed in 6.75×10^{-5} M hemin solution at pH 7.0 for 8 h, (b) $\{CS/HA\}_5$−Mb films after the $\{CS/HA\}_5$ films were immersed in 5.6×10^{-5} M Mb solution at pH 5.0 for 6 h, (c) $\{CS/HA\}_5$−Hb films after the $\{CS/HA\}_5$ films were immersed in 1.5×10^{-5} M Hb solution at pH 5.0 for 12 h, and (d) $\{CS/HA\}_5$−Cat films after the $\{CS/HA\}_5$ films were immersed in 2.1×10^{-5} M Cat solution at pH 5.0 for 10 h. (B) Effect of the immersing time on the surface concentration of electroactive species (Γ*) for (a) $\{CS/HA\}_5$−hemin, (b) $\{CS/HA\}_5$−Mb, (c) $\{CS/HA\}_5$−Hb, and (d) $\{CS/HA\}_5$−Cat films measured in pH 7.0 buffers at 0.2 V s^{-1}.

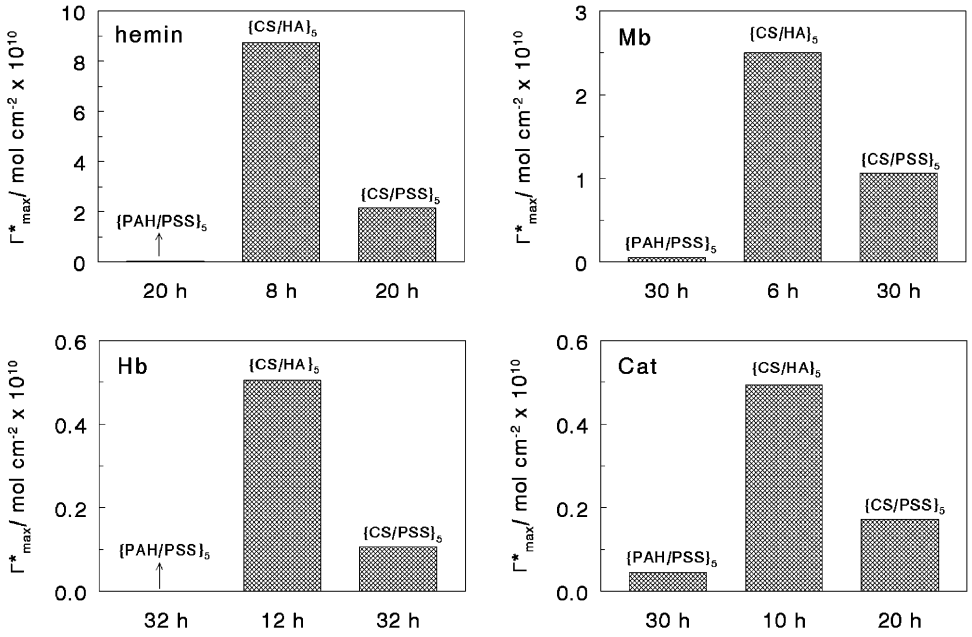

Figure 9. The maximum surface concentration of electroactive species (Γ^*_{max}) for various films measured in pH 7.0 buffers at 0.2 V s^{-1}. The time marked in *X*-axis is the corresponding time, t_{max}, when the steady-state begins to reach.

The swelling of the three types of PEM films in pure water was investigated quantitatively by QCM. After the PEM films with $n = 5$ were immersed in water for 6 h, the films were taken out of the water, and the frequency of swollen films was tested in air by QCM. Comparing the frequency of swollen films with that of dry films before the immersion, the swelling percentage can be estimated according to the formula: swelling percentage = (mass of swollen films − mass of dry films)/mass of dry films × 100%. The swelling percentage of $\{CS/HA\}_5$, $\{CS/PSS\}_5$, and $\{PAH/PSS\}_5$ films was 298%, 177%, and 28%, respectively, showing a sequence of $\{CS/HA\}_5 > \{CS/PSS\}_5 > \{PAH/PSS\}_5$. This order of sequence is in good agreement with that of the porosity or permeability for the films demonstrated in Figure 7.

SEM top views of $\{CS/HA\}_7$, $\{CS/PSS\}_7$, and $\{PAH/PSS\}_7$ films assembled on Au substrates under the used conditions showed that all three types of PEM films had rough morphology with particle aggregation and lots of holes or cavities inside (Supporting Information Figure S4). While the quantitative estimation and differentiation in morphology for the three types of PEM films were difficult, qualitatively speaking, the $\{CS/HA\}_7$ films seemed to show less aggregation than other films and have more small holes and cavities in the structure. The rough surface with small pores for $\{CS/HA\}_n$ films was also observed by atomic force microscopy (AFM) in the literature.[8,18a,19b,20a]

5. Comparison of Incorporation Behaviors of Mb with Hemin, Hb, and Cat into PEM films. To further investigate and understand the loading behavior of $\{CS/HA\}_n$ films, two other heme protein or enzyme, Hb and Cat, were used as probes to be loaded into the films. The dimension of Hb is $6.5 \times 5.5 \times 5.0$ nm,[38] and the average diameter of Cat is about 9.0 nm,[39] both larger than that of Mb (2.5 nm × 3.5 nm × 4.5 nm[40]). In addition, a much smaller molecule, hemin, was also chosen as a probe in loading experiments for comparison.

Not only Mb but also larger-sized Hb and Cat could be loaded into the $\{CS/HA\}_5$ films assembled on the PG electrode surface, and all protein-loaded $\{CS/HA\}_5$ films demonstrated a well-defined and quasireversible CV peak pair (Figure 8A), characteristic of protein heme Fe^{III}/Fe^{II} redox couples.[33] The $\{CS/HA\}_5$−hemin film electrodes also showed the CV peak pair for Fe^{III}/Fe^{II} couple at −0.37 V, close to that of $\{CS/HA\}_5$−Mb and $\{CS/HA\}_5$−Hb films at −0.33 V, while Cat-loaded $\{CS/HA\}_5$ films demonstrated the pair of peaks at −0.46 V. The different peak positions for different $\{CS/HA\}_5$-protein films indicate that the proteins with the same redox center may not have the same formal potential in the same microenvironment, as also observed in the previous work.[41] This also suggests

that the electrochemical responses we observed for $\{CS/HA\}_5$−protein films are not from the released heme prosthetic groups out of the protein polypeptide pockets, and that the proteins loaded in the PEM films do not denature.

The dependence of surface concentrations of electroactive species (Γ^*) on the different loading time (t) for $\{CS/HA\}_5$ films is shown in Figure 8B. While the difference of CV peak areas (Q) for Mb, Hb, and Cat systems in Figure 8A was not obvious, when the Q values were converted to Γ^* values according to $\Gamma^* = Q/(nFA)$,[34] the Mb system showed a much larger Γ^* than that of the Hb or Cat system (Figure 8B), since the number of electrons transferred (n) equals 1 for Mb, much smaller than 4 for Hb and Cat. At the same t, Γ^* displayed the sequence of $\{CS/HA\}_5$−hemin > $\{CS/HA\}_5$−Mb > $\{CS/HA\}_5$−Hb > $\{CS/HA\}_5$−Cat, in agreement with the reverse sequence of molecular size of loaded species (hemin < Mb < Hb < Cat). It is understandable that the larger-sized species would enter into and diffuse through the films with more difficulty.

These four kinds of electroactive species with different sizes were also loaded into $\{CS/PSS\}_5$ and $\{PAH/PSS\}_5$ films and then tested by CV. The values of maximum surface concentration of electroactive species (Γ^*_{max}) at the steady state and the corresponding t_{max} for different film systems were obtained and compared in Figure 9. Compared with $\{CS/PSS\}_5$ and $\{PAH/PSS\}_5$ films, $\{CS/HA\}_5$ films displayed the best loading capability toward all species, such as the largest Γ^*_{max} and the minimum t_{max} values. Among the three PEM films, the $\{PAH/PSS\}_5$ films always showed the lowest loading ability toward all these species and could not even absorb hemin and Hb molecules at all.

Discussion

Proteins, such as Mb, can be adsorbed on a polyelectrolyte surface of either opposite or like charges.[4d,42,43] In the present work, the first question is, for $\{CS/HA\}_n$ layer-by-layer films, what is the main loading mode toward Mb, adsorption or "absorption". The results demonstrate that the Mb molecules in the loading solution are not only adsorbed onto the surface of $\{CS/HA\}_n$ films but also "absorbed" or incorporated into the bulk films, and the latter is mainly responsible for the electrochemical response of Mb for the films. The following three arguments support this point of view: (1) If the surface adsorption were the only mode for Mb loading, the adsorption amount of Mb on the surface of $\{CS/HA\}_n$ films should have remained the same when n increased. However, the fact is, both Γ^* measured by CV and Γ estimated by QCM increase with n under suitable conditions (Figures 2B and 3). (2) Taking $\{CS/HA\}_7$ films with $n = 7$ as an example, the nominal thickness of the films is about 80 nm according to the QCM results.[27] Considering the mixing or interpenetration of neighboring layers in assembly, the actual thickness of $\{CS/HA\}_7$ films would be less than this value. Nevertheless, the thickness of the films should still be in the range of a few tens of nanometers even without considering the film swelling. It is impossible for Mb adsorbed on the film surface to exchange electrons with the underlying PG electrode through such a long distance, since electrons can only tunnel across a few nanometers.[44] The CV response of $\{CS/HA\}_7$−Mb films (Figure 2A) must be mainly attributed to the "absorbed" Mb inside the films. (3) The CV peak currents or Γ^* of $\{CS/HA\}_n$−Mb films are nearly independent of the surface charge of the films (Figure S1), also suggesting that the electroactive Mb molecules are mainly from the interior of the films.

Positively charged Mb at pH 5.0 demonstrates more loading amount than negatively charged Mb at pH 9.0 and neutral Mb at pH 7.0 from Mb solutions under the same conditions (Figure S1), implying that the electrostatic interaction between Mb and the components of $\{CS/HA\}_n$ films may be the main driving force for the loading. While the exact explanation and the detailed mechanism for these phenomena are not very clear yet, negatively charged HA inside the $\{CS/HA\}_n$ films probably plays a more important role in loading Mb than positively charged CS. At pH 5.0, negative HA in the films tends to attract more amounts of oppositely charged Mb, while at pH 9.0, the repulsion between HA and Mb with the same negative charges may result in the less loading amount. Since the negative charges of the HA component inside the $\{CS/HA\}_n$ films are mainly responsible for the loading of Mb, the loading amount of Mb shows little relationship with the charge or component of the outermost layer of the films (Figure S1). Similar phenomena were also observed for other exponentially growing PEM films,[24,25] where the loading amount of ferricyanide or ferrocyanide in the films was irrespective of the sign of the surface charge of the films, and only one component of the PEM films played a major role in incorporation of $Fe(CN)_6^{3-/4-}$.

While the electrostatic interaction may be the main driving force for Mb to be loaded into $\{CS/HA\}_n$ films, other interactions, such as hydrophobic force and hydrogen bonding, cannot be ruled out completely. To support this viewpoint, a comparison experiment was designed and performed with two small and hydrophilic ions, $Fe(CN)_6^{3-}$ and $Ru(NH_3)_6^{3+}$, as the probes. When immersed in $K_3Fe(CN)_6$ solution, the $\{CS/HA\}_5$ film electrode demonstrated a quasireversible CV peak pair for $Fe(CN)_6^{3-/4-}$ couple (not shown). However, after the ferricyanide-loaded $\{CS/HA\}_5$ films were transferred in pH 7.0 buffers containing no $K_3Fe(CN)_6$, only a small peak pair at about 0.15 V was observed (Supporting Information Figure S5A, curve a). The CV response quickly decreased with the soaking time and almost disappeared in 1 h (Figure S5A, curve b). A similar phenomenon was observed for $Ru(NH_3)_6^{3+}$-loaded $\{CS/HA\}_5$ films (Figure S5B). These results suggest that the loaded small ions in the $\{CS/HA\}_5$ films are almost completely unloaded in blank buffers in 1 h, and these highly hydrophilic ions cannot "stay" stably inside the films, irrespective of charge situation of either the probes or the outermost layers. On the contrary, $\{CS/HA\}_n$−Mb films demonstrated excellent stability in blank buffers. Even after 10 days of soaking in buffers, the CV of $\{CS/HA\}_5$−Mb films kept almost identical with the initial one (Figure S5C). The hydrophobic interaction or/and hydrogen bonding between Mb and CS/HA in the films must be an important driving force in Mb loading and plays a key role in stabilizing the films in blank buffers.

For the mechanism of electron transfer of Mb in $\{CS/HA\}_n$−Mb films, it is almost impossible for Mb to physically diffuse to the electrode surface through the film phase and then exchange electrons with underlying electrodes in the time scale of CV scans, since physical diffusion of macromolecular Mb in the films would take several hours (Figure 2B). It is thus most probable for Mb to take the electron-hopping or self-exchange mechanism[45] to transfer electrons in the films. That is, the electron exchange between two neighboring Mb molecules inside the films would be the main mode of charge transport in $\{CS/HA\}_n$−Mb films. In electron hopping, to compensate for the charge alteration caused by electron transfer and keep the electroneutralization of the films, the transportation of counterions in the film phase not only is necessary but also may become a limiting factor.[45] The transport of counterions

from solution into the films and within the film phase depends on the permeability of the films, and the film permeability decreases as the film thickness increases (Figures 7B and S3). This would explain why the fraction of electroactive Mb in $\{CS/HA\}_n$ films ($\Gamma^*_{max}/\Gamma_{max}$) decreases drastically with the film thickness, and the electroactive Mb can only extend to $n = 7$ and no longer increase when $n > 7$ (Figure 3). The result suggests that only those Mb molecules in a few bilayers closest to the electrode surface can display electrochemical activity, which is also a character of electron-hopping when counterion transportation becomes a limiting factor, as also observed in other protein layer-by-layer films.[4] Of course, the above explanation may not be perfect in elucidation of electron transfer for $\{CS/HA\}_n$−Mb films and only provides one possibility. The further study to this direction is underway in this laboratory.

For the loading of Mb, Γ^* shows the sequence of $\{CS/HA\}_n > \{CS/PSS\}_n > \{PAH/PSS\}_n$, and $\{CS/HA\}_n$ films demonstrate the best loading capability (Figure 6). The loading amount and efficiency for a specific PEM film is also influenced by the size of loading species (Figure 8), and the smaller-sized species demonstrates larger Γ^*_{max} for $\{CS/HA\}_n$ films (Figure 9). For any probe studied in this work, the Γ^*_{max} shows the same sequence of $\{CS/HA\}_n > \{CS/PSS\}_n > \{PAH/PSS\}_n$. This is consistent with the sequence of these films in permeability, as shown by EIS and RDV studies (Figures 7 and S3). The permeability of the PEM films seems to have a close correlation with their swelling properties.[12a] As demonstrated by QCM results, the swelling or water-absorption ability of the PEM films displays the same sequence as that of permeability and loading capability. The different swelling and permeation properties of different PEM films are probably related to the structure feature of the film components, especially to the charge densities of the PEM constituents.[12−14] The chemical structures of the polyelectrolytes used in this work are shown in Figure 1. CS and PAH contain one positive charge per 11 and 4 non-hydrogen atoms, respectively, indicating that CS has lower charge density than PAH. Similarly, HA and PSS have one negative charge per 26 and 12 non-hydrogen atoms, respectively.[12a] If the charge density index of the films is defined as the sum of the numbers of non-hydrogen atoms for one positive/negative charge of the polycation/polyanion that constitute the layer-by-layer films, the charge density index of the films shows the sequence of $\{CS/HA\}_n$ (37) > $\{CS/PSS\}_n$ (23) > $\{PAH/PSS\}_n$ (16), in good agreement with that of swelling and permeation properties for the films. Since $\{CS/HA\}_n$ films have the larger index and lower charge density than the other PEM films, the $\{CS/HA\}_n$ films have the fewer ionic cross-link pairs and the looser film structure. The relatively rigid structure of the pyranose ring in CS and HA monomers may also play an important role in the formation of a looser structure of $\{CS/HA\}_n$ films. $\{CS/HA\}_n$ films are a kind of exponentially growing PEM film,[12b,19,20] while $\{CS/PSS\}_n$ and $\{PAH/PSS\}_n$ films were reported to grow linearly.[46,47] It has been shown that the exponential growth is due to the diffusion "in" and "out of" the entire PEM films during the deposition of at least one of the components used for the film construction.[48] These films are thus much less dense and more permeable than the linearly growing ones.[24,25] It is due to the unique structure and properties of CS and HA that the $\{CS/HA\}_n$ films assembled by these two polysaccharides swell to a greater extent in aqueous solution than the other PEM films. The higher swelling capability of $\{CS/HA\}_n$ films may lead to better permeability for soluble probes and a higher loading amount of Mb.

The ionic strength has a significant influence on the swelling and permeability of the PEM films as shown in Figure S3 in this work and also as reported in the literature.[49−52] Higher ionic strength in solution weakens the ionic bonds between oppositely charged polyelectrolytes that hold the layers together and allows the formation of more loops and trains in PEM films, which may change the layer structure of the films with more water-filled cavities, and usually results in the loosening of film structure and the increase of film swelling degree and permeability. Thus, with a higher concentration of NaCl in the Mb loading solution, more Mb molecules could be absorbed or loaded into the $\{CS/HA\}_n$ films (Figure 4). Moreover, while the total amount of Mb (Γ) for $\{CS/HA\}_3$−Mb films does not change with the NaCl concentration in the exposure solution, the amount of electroactive Mb (Γ^*) in the films increases with C_{NaCl} (Figure S2), indicating that the ratio of Γ^*/Γ or the fraction of electroactive Mb would increase with ionic strength. The higher concentration of salt in the exposure solution may cause the greater swelling extent of $\{CS/HA\}_3$−Mb films and lead to the higher film permeability, thus facilitating the counterion transportation within the films and making more amounts of Mb electroactive in electron-hopping. In addition, the great effect of ionic strength on loading behavior of $\{CS/HA\}_n$ films toward Mb also confirms that electrostatic interaction plays an important role in the loading processes.

Conclusions

The understanding of the loading mechanism of PEM films toward proteins is of prime importance in the design of protein-loaded PEM films with biological activities. In this paper, the loading behavior of $\{CS/HA\}_n$ layer-by-layer films toward Mb is studied and compared with $\{CS/PSS\}_n$ and $\{PAH/PSS\}_n$ films. Among the three PEM films, $\{CS/HA\}_n$ films demonstrate the best swelling capability and permeability, which results in the highest loading amount of Mb and the shortest loading time under the suitable conditions. The best swelling and permeation properties of $\{CS/HA\}_n$ films are most probably related to the lowest charge density of the films and the unique structure of CS and HA. The excellent property of $\{CS/HA\}_n$ films in Mb loading may make the films become a good candidate in fabricating protein-loaded PEM films. The protein-loaded PEM films not only may provide a general approach in immobilization of proteins and open up great perspectives in design of the new bioactive surface but also may offer a new way to construct the electrochemical biosensors based on the direct electrochemistry of enzymes.

Acknowledgment. The financial support from the National Natural Science Foundation of China (NSFC 20475008 and 20275006) is acknowledged.

Supporting Information Available: Five figures showing CVs of $\{CS/HA\}_3$−Mb and $\{CS/HA\}_3/CS$−Mb films prepared from Mb loading solution at different pHs, effect of the NaCl concentration in exposure solution on Γ^* for $\{CS/HA\}_3$−Mb films, influence of the number of bilayers (n) on RDV reduction limiting current (I_{lim}) of $K_3Fe(CN)_6$ in KCl solutions of different concentrations for $\{CS/HA\}_n$, $\{CS/PSS\}_n$, and $\{PAH/PSS\}_n$ films, SEM top views of $\{CS/HA\}_7$, $\{CS/PSS\}_7$, and $\{PAH/PSS\}_7$ films, and CVs of $\{CS/HA\}_5$−$Fe(CN)_6^{3-}$, $\{CS/HA\}_5$−$Ru(NH_3)_6^{3+}$, and $\{CS/HA\}_5$−Mb film electrodes with immediate scan and with scan after some time of soaking in blank buffers. This material is available free of charge via the Internet at http://pubs.acs.org.

References and Notes

(1) Decher, G. *Science* **1997**, *277*, 1232−1237.

(2) (a) Lvov, Y. In *Protein Architecture: Interfacing Molecular Assemblies and Immobilization Biotechnology*; Lvov, Y., Mohwald, H., Eds.; Marcel Dekker: New York, 2000; pp 125−167. (b) Lvov, Y. In *Nanostructured Materials, Micelles and Colloids*; Nalwa, R. W., Ed.; Handbook of Surfaces and Interfaces of Materials 3; Academic Press: San Diego, 2001; pp 170−189.

(3) (a) Lvov, Y.; Lu, Z.; Schenkman, J. B.; Zu, X.; Rusling, J. F. *J. Am. Chem. Soc.* **1998**, *120*, 4073−4080. (b) Lvov, Y.; Munge, B.; Giraldo, O.; Ichinose, I.; Suib, S.; Rusling, J. F. *Langmuir* **2000**, *16*, 8850−8857.

(4) (a) Ma, H.; Hu, N.; Rusling, J. F. *Langmuir* **2000**, *16*, 4969−4975. (b) He, P.; Hu, N.; Zhou, G. *Biomacromolecules* **2002**, *3*, 139−146. (c) Zhou, Y.; Li, Z.; Hu, N.; Zeng, Y.; Rusling, J. F. *Langmuir* **2002**, *18*, 8573−8579. (d) He, P.; Hu, N. *J. Phys. Chem. B* **2004**, *108*, 13144−13152.

(5) Chapin, M. F.; Bucke, C. *Enzyme Technology*; Cambridge University Press: Cambridge, U.K., 1990.

(6) Armstrong, F. A.; Wilson, G. S. *Electrochim. Acta* **2000**, *45*, 2623−2645.

(7) Salloum, D. S.; Schlenoff, J. B. *Biomacromolecules* **2004**, *5*, 1089−1096.

(8) Liu, Y.; Lu, H.; Zhong, W.; Song, P.; Kong, J.; Yang, P.; Girault, H. H.; Liu, B. *Anal. Chem.* **2006**, *78*, 801−808.

(9) Weidinger, I. M.; Murgida, D. H.; Dong, W.; Mohwald, H.; Hildebrandt, P. *J. Phys. Chem. B* **2006**, *110*, 522−529.

(10) (a) Lvov Y.; Antipov, A.; Mamedov, A.; Mowald, H.; Sukhorukov, G. B. *Nano Lett.* **2001**, *1*, 125−128. (b) Tiourina, O. P.; Antipov, A. A.; Sukhorukov, G. B.; Larionova, N. I.; Lvov, Y.; Mohwald, H. *Macromol. Biosci.* **2001**, *1*, 209−214. (c) Tiourina, O. P.; Sukhorukov, G. B. *Int. J. Pharm.* **2002**, *242*, 155−161. (d) Balabushevich, G. N.; Tiourina, O. P.; Volodkin, D. V.; Larionova, N. I.; Sukhorukov, G. B. *Biomacromolecules* **2003**, *4*, 1191−1197.

(11) Schwinte, P.; Voegel, J.-C.; Picart, C.; Haikel, Y.; Schaaf, P.; Szalontai, B. *J. Phys. Chem. B* **2001**, *105*, 11906−11916.

(12) (a) Miller, M. D.; Bruening, M. L. *Chem. Mater.* **2005**, *17*, 5375−5381. (b) Miller, M. D.; Bruening, M. L. *Langmuir* **2004**, *20*, 11545−11551. (c) Stanton, B. W.; Harris, J. J.; Miller, M. D.; Bruening, M. L. *Langmuir* **2003**, *19*, 7038−7042.

(13) (a) Krasemann, L.; Tieke, B. *Mater. Sci. Eng., C* **1999**, *C8*−*C9*, 513−518. (b) Krasemann, L.; Tieke, B. *Langmuir* **2000**, *16*, 287−290.

(14) (a) Sun, Q.; Tong, Z.; Wang, C.; Ren, B.; Liu, X.; Zeng, F. *Polymer* **2005**, *46*, 4958−4966. (b) Burke, S. E.; Barrett, C. J. *Macromolecules* **2004**, *37*, 5375−5384.

(15) Lapcik, L., Jr.; Lapcik, L.; De Smedt, S.; Demeester, J.; Chabrecek, P. *Chem. Rev.* **1998**, *98*, 2663−2684.

(16) Jentsch, H.; Pomowski, R.; Kundt, G.; Gocke, R. *J. Clin. Periodontol.* **2003**, *30*, 159−164.

(17) Ikinci, G.; Senel, S.; Akincibay, H.; Kas, S.; Ercis, S.; Wilson, C. G.; Hincal, A. A. *Int. J. Pharm.* **2002**, *235*, 121−127.

(18) (a) Thierry, B.; Winnik, F. M.; Merhi, Y.; Silver, J.; Tabrizian, M. *Biomacromolecules* **2003**, *4*, 1564−1571. (b) Thierry, B.; Winnik, F. M.; Merhi, Y.; Tabrician, M. *J. Am. Chem. Soc.* **2003**, *125*, 7494−7495.

(19) (a) Kujawa, P.; Badia, A.; Winnik, F. M. *Polym. Mater. Sci. Eng.* **2004**, *90*, 192−193. (b) Kujawa, P.; Moraille, P.; Sanchez, J.; Badia, A.; Winnik, F. M. *J. Am. Chem. Soc.* **2005**, *127*, 9224−9234.

(20) (a) Richert, L.; Lavalle, P.; Payan, E.; Zheng, X. S.; Prestwich, G. D.; Stoltz, J. F.; Schaaf, P.; Voegel, J.-C.; Picart, C. *Langmuir* **2004**, *20*, 448−458. (b) Etienne, O.; Schneider, A.; Taddei, C.; Richert, L.; Schaaf, P.; Voegel, J.-C.; Egles, C.; Picart, C. *Biomacromolecules* **2005**, *6*, 726−733.

(21) Feng, Q.; Zeng, G.; Yang, P.; Wang, C.; Cai, *J. Colloids Surf. A: Physicochem. Eng. Aspects* **2005**, *257*−*258*, 85−88.

(22) Lu, D.; Meng, S.; Zhong, W.; Du, Q.; Gong, L.; Liu, J.; Dusan, B. *Chin. Sci. Bull.* **2005**, *50*, 2809−2816.

(23) Croll, T. I.; O'Connor, A. J.; Stevens, G. W.; Cooper-White, J. J. *Biomacromolecules* **2006**, *7*, 1610−1622.

(24) Hubsch, E.; Fleith, G.; Fatisson, J.; Labbe, P.; Voegel, J.-C.; Schaaf, P.; Ball, V. *Langmuir* **2005**, *21*, 3664−3669.

(25) Noguchi, T.; Anzai, J. *Langmuir* **2006**, *22*, 2870−2875.

(26) Huang, H.; Hu, N.; Zeng, Y.; Zhou, G. *Anal. Biochem.* **2002**, *308*, 141−151.

(27) Liu, H.; Hu, N. *J. Phys. Chem. B* **2006**, *110*, 11494−11502.

(28) Sauerbrey, G. *Z. Phys.* **1959**, *155*, 206−222.

(29) Lvov, Y.; Ariga, K.; Ichinose, I.; Kunitake, T. *J. Am. Chem. Soc.* **1995**, *117*, 6117−6123.

(30) Serizawa, T.; Kamimura, S.; Kawanishi, N.; Akashi, M. *Langmuir* **2002**, *18*, 8381−8385.

(31) (a) Denuziere, A.; Ferriera, D.; Domard, A. *Carbohydr. Polym.* **1996**, *29*, 317−323. (b) Rinaudo, M.; Milas, M.; Le Dung, P. *Int. J. Biol. Macromol.* **1993**, *15*, 281−285.

(32) Bellelli, A.; Antonini, G.; Brunori, M.; Springer, B. A.; Sligar, S. J. *J. Biol. Chem.* **1990**, *265*, 18898−18901.

(33) (a) Rusling, J. F.; Zhang, Z. In *Biomolecules, Biointerfaces, and Applications*; Nalwa, R. W., Ed.; Handbook of Surfaces and Interfaces of Materials 5; Academic Press: San Diego, 2001; pp 33−71. (b) Rusling, J. F. *Acc. Chem. Res.* **1998**, *31*, 363−369.

(34) Murray, R. W. In *Electroanalytical Chemistry*; Bard, A. J., Ed.; Marcel Dekker: New York, 1984; Vol. 13, pp 191−368.

(35) (a) Theorell, H.; Ehrenberg, A. *Acta Chem. Scand.* **1951**, *5*, 823−848. (b) George, P.; Hanania, G. I. H. *Biochem. J.* **1953**, *55*, 236−243.

(36) Katz, E.; Willner, I. *Electroanalysis* **2003**, *15*, 913−947.

(37) (a) Sabatani, E.; Rubinstein, I. *J. Phys. Chem.* **1987**, *91*, 6663−6669. (b) Sabatani, E.; Cohen-Boulakia, J.; Bruening, M.; Rubinstein, I. *Langmuir* **1993**, *9*, 2974−2981.

(38) Weissbluth, M. *Molecular Biology: Biochemistry and Biophysics*; Springer-Verlag: New York, 1974; Vol. 15.

(39) Lvov, Y.; Ariga, K.; Ichinose, I.; Kunitake, T. *Thin Solid Films* **1996**, *284*, 797−801.

(40) Kendrew, J.; Phillips, D.; Stone, V. *Nature (London)* **1960**, *185*, 422−427.

(41) (a) Shen, L.; Hu. N. *Biochim. Biophys. Acta*—Bioenerg. **2004**, *1608*, 23−33. (b) Li, M.; He, P.; Hu. N. *Biochim. Biophys. Acta*—Proteins Protem. **2005**, *1749*, 43−51. (c) Lu, H.; Yang, J.; Rusling, J. F.; Hu, N. *Electroanalysis* **2006**, *18*, 379−390.

(42) (a) Ladam, G.; Gergely, C.; Senger, B.; Decher, G.; Voegel, J.-C.; Schaaf, P.; Cuisinier, F. J. G. *Biomacromolecules* **2000**, *1*, 674−687. (b) Ladam, G.; Schaaf, P.; Cuisinier, F. J. G.; Decher, G.; Voegel, J.-C. *Langmuir* **2001**, *17*, 878−882. (c) Ladam, G.; Schaaf, P.; Decher, G.; Voegel, J.-C.; Cuisinier, F. J. G. *Biomol. Eng.* **2002**, *19*, 273−280.

(43) Schenkman, J. B.; Jansson, I.; Lvov, Y. M.; Rusling, J. F.; Boussaad, S.; Tao, N. J. *Arch. Biochem. Biophys.* **2001**, *385*, 78−87.

(44) Page, C. C.; Moser, C. C.; Chen, X.; Dutton, P. L. *Nature* **1999**, *402*, 47−52.

(45) Majda, M. In *Molecular Design of Electrode Surfaces*; Murray, R. W., Ed.; Wiley: New York, 1992; pp 159−206.

(46) Caruso, F.; Niikura, K.; Furlong, D. N.; Okahata, Y. *Langmuir* **1997**, *13*, 3422−3426.

(47) Lvov, Y.; Onda, M.; Ariga, K.; Kunitake, T. *J. Biomater. Sci. Polym. Ed.* **1998**, *9*, 345−355.

(48) (a) Picart, C.; Mutterer, J.; Richert, L.; Luo, Y.; Prestwich, G. D.; Schaaf, P.; Voegel, J.-C.; Lavalle, P. *Proc. Natl. Acad. Sci. U.S.A.* **2002**, *99*, 12531−12535. (b) Lavalle, P.; Picart, C.; Mutterer, J.; Gergely, C.; Reiss, H.; Voegel, J.-C.; Senger, B.; Schaaf, P. *J. Phys. Chem. B* **2004**, *108*, 635−648.

(49) Harris, J. J.; Bruening, M. L. *Langmuir* **2000**, *16*, 2006−2013.

(50) (a) Sukhorukov, G. B.; Schmitt, J.; Decher, G. *Ber. Bunsen-Ges. Phys. Chem.* **1996**, *100*, 948−953. (b) Antipov, A. A.; Sukhorukov, G. B.; Mohwald, H. *Langmuir* **2003**, *19*, 2444−2448.

(51) (a) Farhat, T. R.; Schlenoff, J. B. *Langmuir* **2001**, *17*, 1184−1192. (b) Dubas, S. T.; Schlenoff, J. B. *Langmuir* **2001**, *17*, 7725−7727.

(52) Burke, S. E.; Barrett, C. J. *Biomacromolecules* **2005**, *6*, 1419−1428.